MICROBIAL METABOLIC EXCHANGE IN 3D

SUPPLEMENTARY INFORMATION

Jeramie Watrous[1,2*], Vanessa V. Phelan[2*], Cheng-Chih Hsu[1*], Wilna Moree[2], Brendan M. Duggan[2], Theodore Alexandrov[2,3†] and Pieter C. Dorrestein[1,2,4,5†]

[1]: Department of Chemistry and Biochemistry, University of California, San Diego, La Jolla, CA, USA
[2]: Skaggs School of Pharmacy and Pharmaceutical Sciences, University of California, San Diego, La Jolla, CA, USA
[3]: Center for Industrial Mathematics, University of Bremen, Bremen, Germany
[4]: Department of Pharmacology, University of California, San Diego, La Jolla, CA, USA
[5]: Center for Marine Biotechnology and Biomedicine, Scripps Institution of Oceanography, La Jolla, CA, USA
*: Authors contributed equally
†: To whom correspondence should be addressed: For interspecies interactions, the experiments and development of the idea pdorrestein@ucsd.edu (Pieter Dorrestein) and for the 3D reconstruction theodore@math.uni-bremen.de (Theodore Alexandrov)

Table of Contents

Supplementary Methods – Generation of 3D Models

Generation of 3D models from MALDI-TOF IMS data

Spectra were exported from the official Bruker spectral format into the mzXML format using the free software CompassXport (Bruker Daltonics, Bremen, Germany). The rest of processing was done using custom made scripts in the MATLAB software (The Mathworks Inc., Natick, MA, USA). Each spectrum was loaded using the "mzxmlread" MATLAB routine (Bioinformatics Toolbox) and binned to 10,000 bins. After normalization to the total ion count, each spectrum was baseline corrected with the "msbackadj" MATLAB routine (Bioinformatics Toolbox) with regression method "pchip", smoothing method "lowess", and window size 200 *m/z*-values. For a given *m/z*-value, a volume dataset, where an intensity value corresponds to a voxel with coordinates (x,y,z), was created as follows. All slices were interpolated onto the same grid of coordinates (x,y), taken from a template slice. This compensates for stretching and shrinking of a slice. Due to rectangular size of a slice, careful alignment of slices placed on a MALDI target plate, and manual selection of slice areas in flexImaging, no registration involving compensation for rotation or non-affine deformation was necessary. For each spectrum, its slice ordinal number was used as its z-coordinate, producing for an *m/z*-value a volume dataset, which was processed prior to visualization as follows. First, abnormally intense spectra, or "hot spots", which are typically observed in MALDI-TOF IMS were removed by computing the 99% or 95% quantile and assigning higher values to the quantile value (so-called quantile filtering). Secondly, the two pixels adjacent to each edge of a slice were skipped to remove non-relevant pixels corresponding to the edge of a slice that were not part of the relevant imaging area; this number of pixels was determined experimentally. Thirdly, the volume data was denoised using the image convolution filter with 3D Gaussian function of span of 5 pixels in all directions. Finally, we improved the contrast by using the 85% quantile filtering. A resulting 3D volume dataset corresponding to an *m/z*-value was visualized using 50%, 75%, and 90% semi-transparent isosurfaces to indicate signal intensity within the 3D model, with the 50% isosurface having highest transparency. Each isosurface was smoothed for better visualization. Given an *m/z*-value, the visualized 3D model highlights spatial regions with 90%, 70%, and 50% relative abundance of a molecular compound of this *m/z*-value.

Supplementary Methods – Purification and characterization of rhamnolipids

Purification of rhamnolipids

Pseudomonas aeruginosa PAO1 was inoculated across 50 ISP2 agar plates by 5 parallel streaks on each plate and were incubated for 4 days at 30 °C. The agar was sliced into small pieces and extracted by immersing the agar pieces in 150 mL of ethyl acetate and shaking for 12 hours at 30 °C. The clear ethyl acetate layer was taken and the solvent removed using a rotor-vaporator (Buchner). The dried crude material was re-dissolved in 2 mL of ethyl acetate and fractionated via a Sephadex LH-20 gel filtration column using a mobile phase of methanol/ethyl acetate (2:1, v/v) at a flow rate of 0.5 mL/min. Each fraction (0.5 ml) was analyzed by MALDI-TOF MS and the fractions containing rhamnolipids (*m/z* 673, 699, and 701) were collected and further purified by HPLC. Compounds were eluted from a Phenomenex Luna C_{18} (250 x 4.6 mm) column using a solvent gradient running from 50% solvent A to 95% solvent A over 30 minutes with flow rate 2 mL/min while collecting 1 mL fractions using an automated fraction collector. Solvent A was H_2O containing 0.1% TFA and solvent B is acetonitrile containing 0.1% TFA. Fractions containing purified rhamnolipids were lyophilized and stored at -20ºC before using for bioassay and structural elucidation. The yields were approximately 200, 30, and 20 µg per plate for rhamnolipids *m/z* 673, 699, and 701, respectively. See supporting figures for MS and NMR spectra.

Preparation for NMR analysis

500 µg of rhamnolipids m/z 673, 699, and 701 were dissolved in 40 µL of CD_3OD for NMR data acquisition. NMR spectra were recorded on a Bruker Avance III 600 MHz spectrometer with 1.7 mm Micro-CryoProbe at 298 K, with standard pulse sequences provided by Bruker. Structures were confirmed by analysis of 1D proton, 2D DQF-COSY, 2D ^{1}H-^{13}C HSQC and 2D ^{1}H-^{13}C HMC spectra. 2D ^{1}H-^{13}C HMBC spectra were recorded with delays corresponding to ^{2}J or ^{3}J H-C coupling constants of 8 Hz and ^{1}J H-C coupling constants of 145 Hz. 2D ^{1}H-^{13}C multiplicity edited HSQC spectra were recorded with delays corresponding to ^{1}J H-C coupling constants of 140 Hz. Spectra were referenced to the methanol methyl resonance at 3.31ppm.

Figure S1: MS data showing blade cleaning procedure efficiency

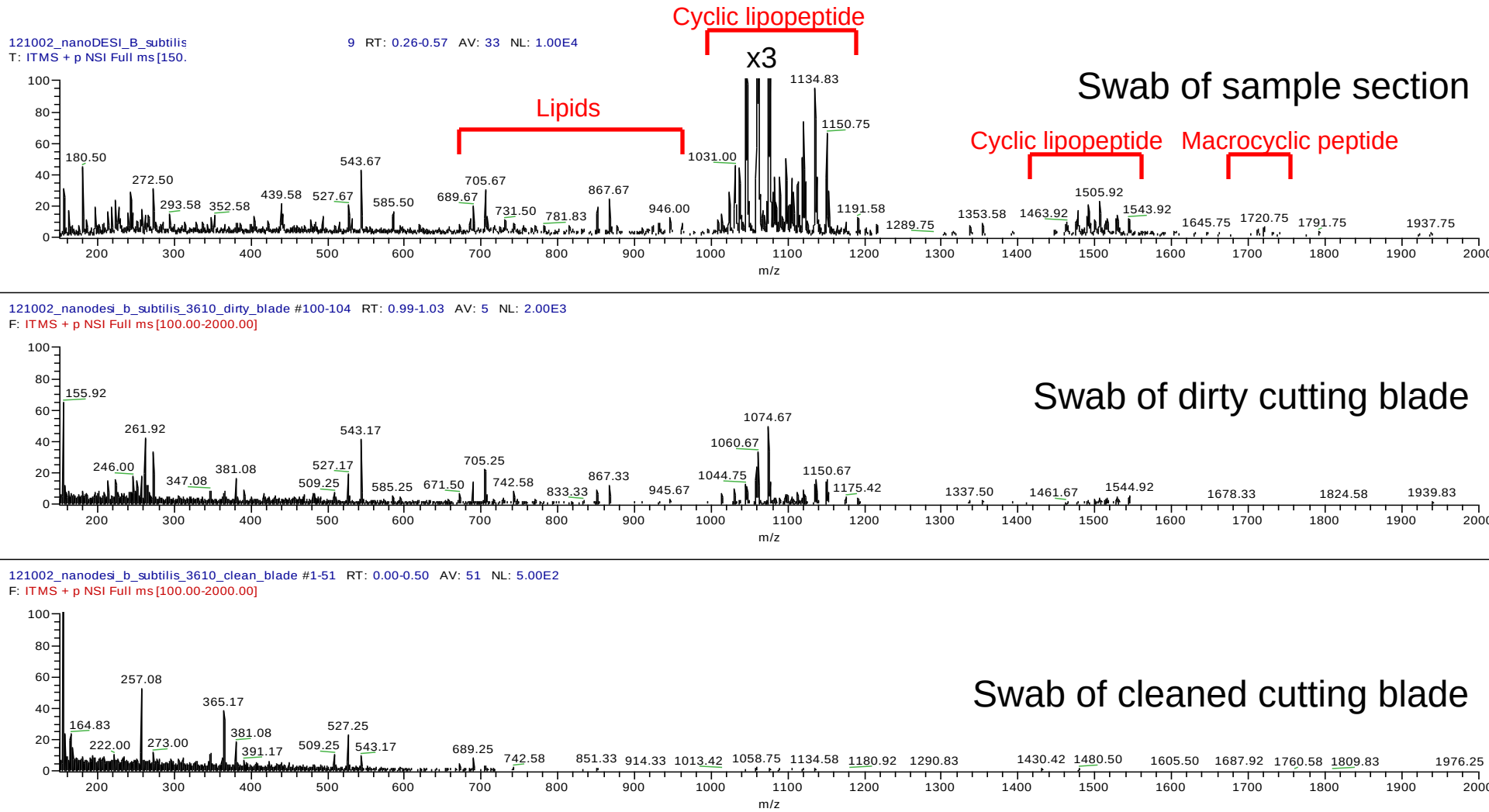

Description: To confirm the efficiency of the cryotome blade cleaning procedure, a sample of *B. subtilis* 3610 was prepared on 8 mm deep agar media according to the procedure described in the main text. This bacteria was chosen due to it producing very high amounts of widely varied metabolites as described in (Watrous *et al*, 2012). Using a new crytome blade, a single cut was made down the middle of the colony. Using a cotton swab, both the freshly cut sample section and the used blade were swabbed. The blade was then cleaned using the procedure described in the main text and swabbed again. The three swabs were extracted with 250μL of 60% ACN:40% Water containing 0.05% Formic Acid and infused into a Thermo LTQ-FT mass spectrometer using the parameters described in the main text. The resulting data shows that metabolites transferred to the cutting blade were sufficiently removed during cleaning.

Figure S2: Additional mass signals from *B. subtilis* PY79 vs. *S. coelicolor* A3(2)

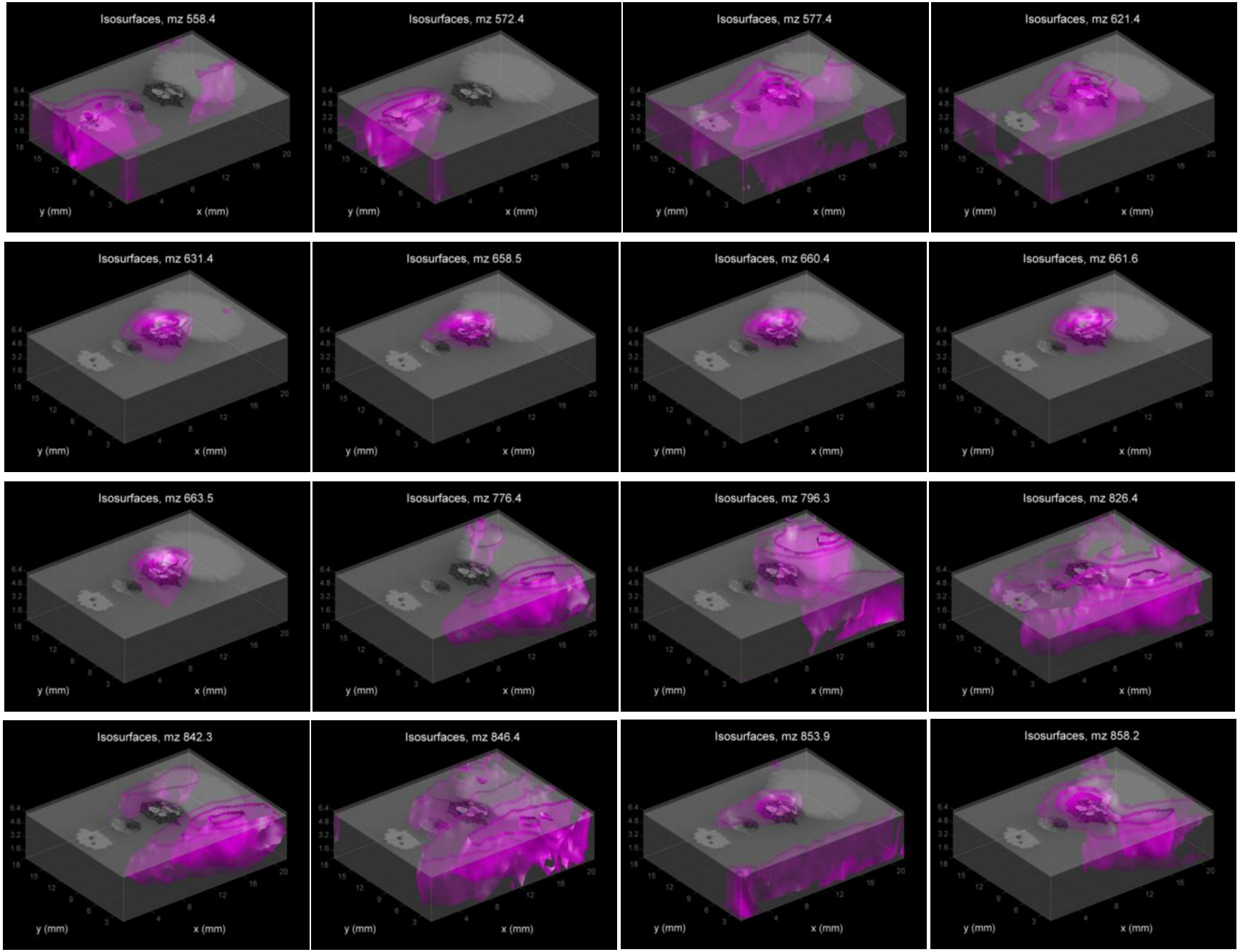

Figure S2: Additional mass signals from *B. subtilis* PY79 vs. *S. coelicolor* A3(2)

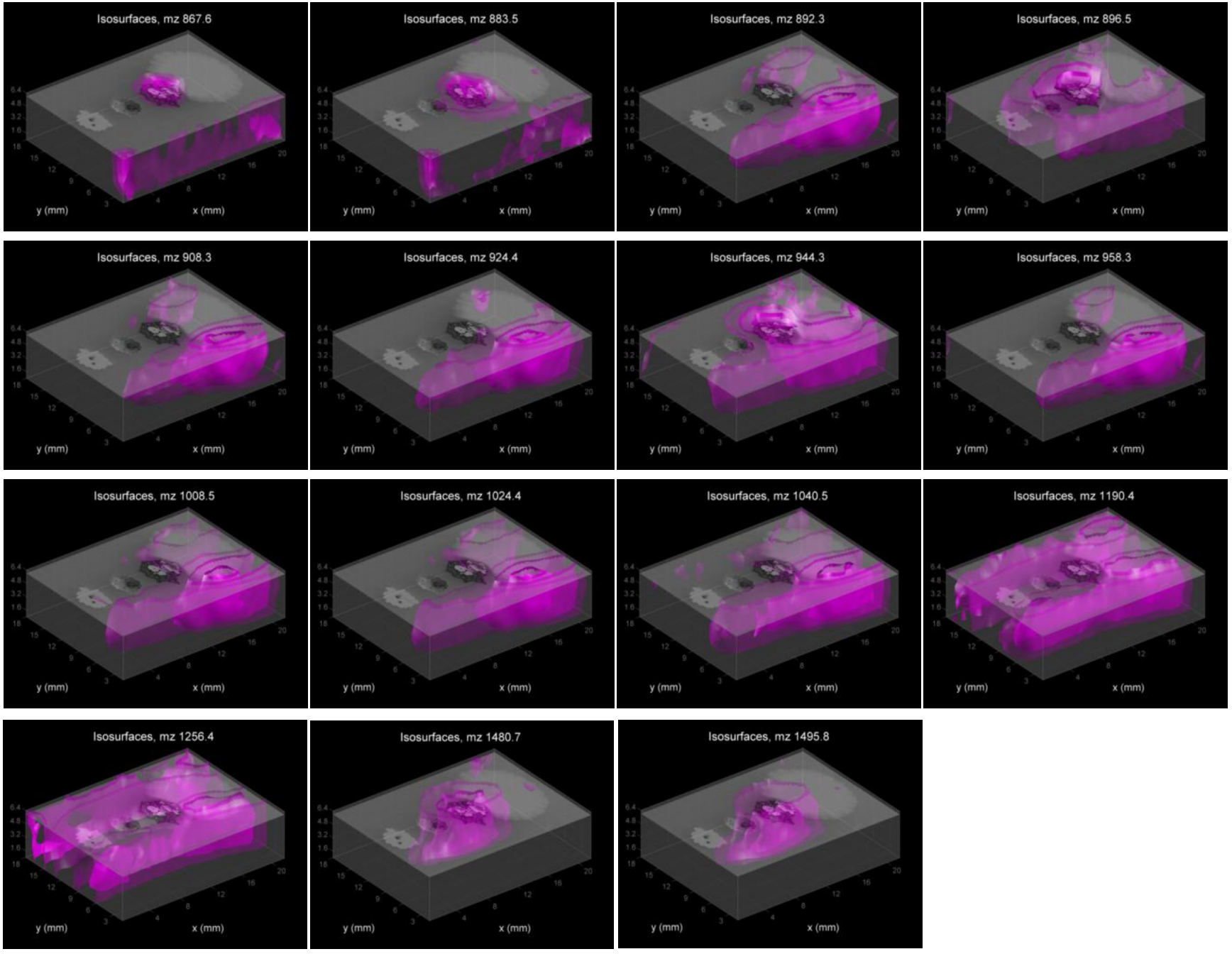

Figure S3: Signal for prodiginine from individual slice from 3D data set

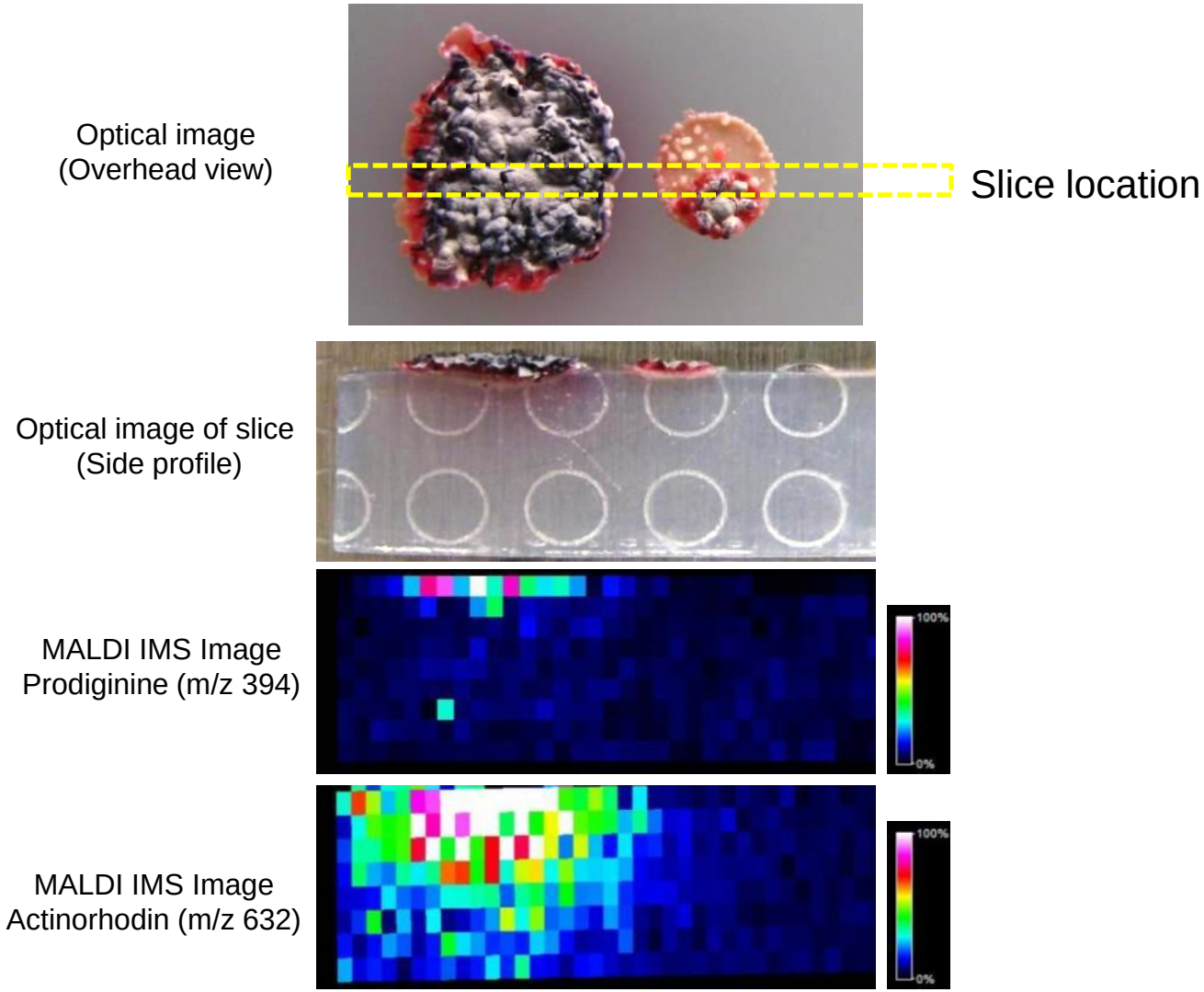

Description: Comparison of MALDI IMS signals for prodiginine (m/z 394) and γ-actinorhodin (m/z 632) from a single cross sectional slice through a Streptomyces coelicolor A3(2) colony. MALDI IMS of the cross sectional slice showed signal for prodiginine localized to the colony while signal for γ-actinorhodin was seen throughout the agar beneath the colony. Scale bar shows percent relative signal intensity throughout the images area.

Figure S4: Additional mass signals from *C. albicans* ySN250 vs. *P. Aeruginosa PAO1*

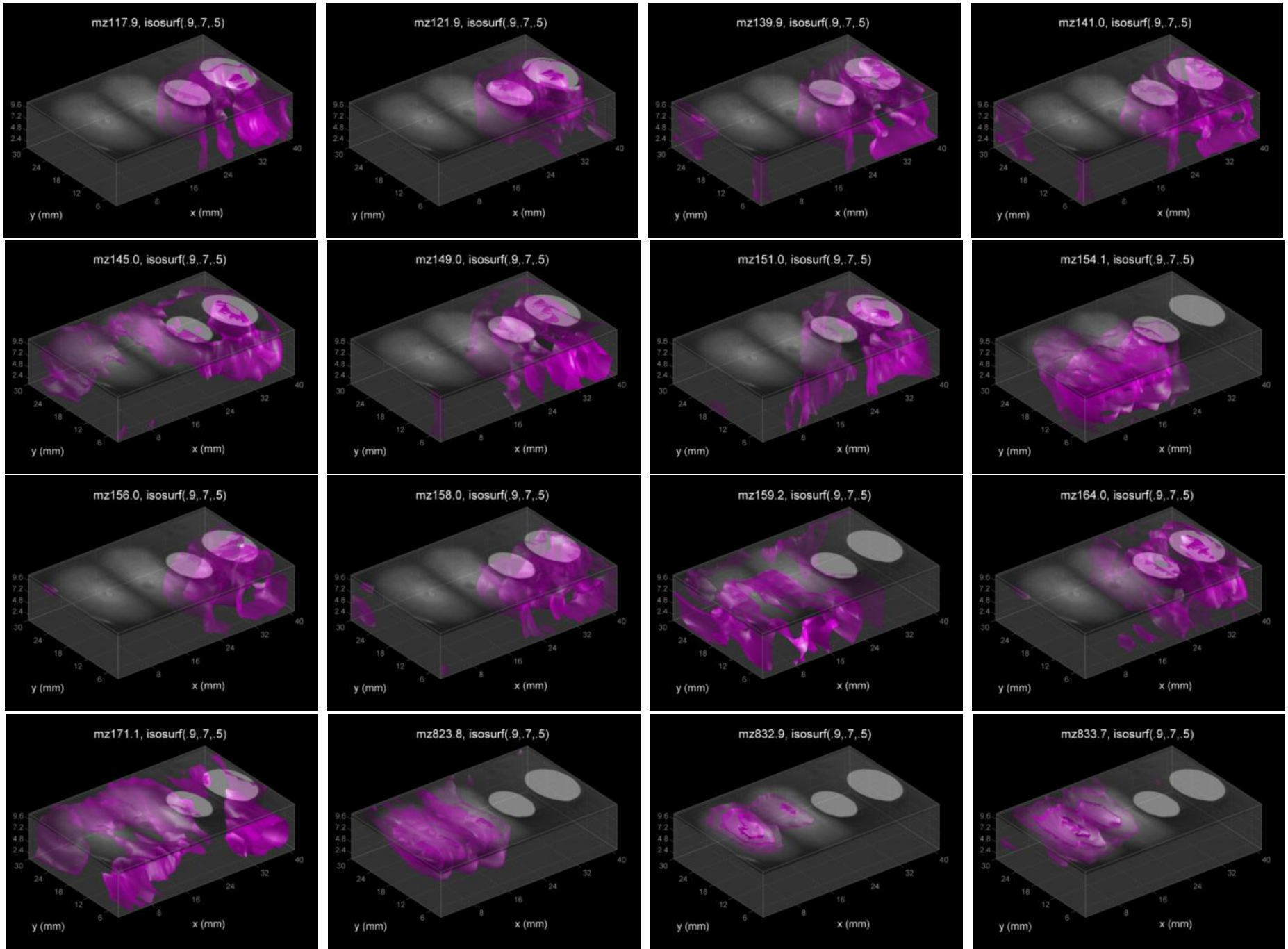

Figure S4: Additional mass signals from *C. albicans* ySN250 vs. *P. Aeruginosa PAO1*

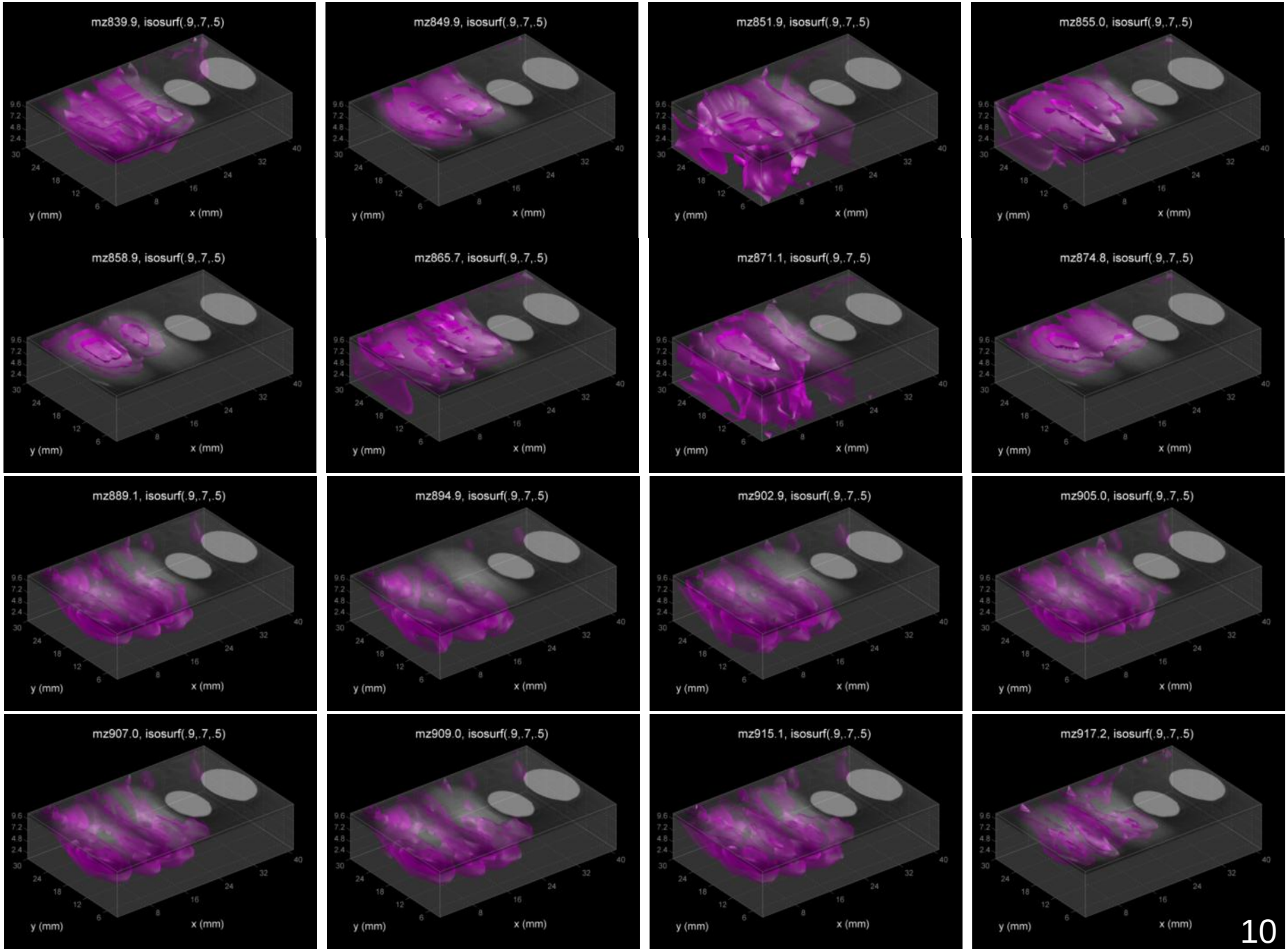

Figure S4: Additional mass signals from *C. albicans* ySN250 vs. *P. Aeruginosa PAO1*

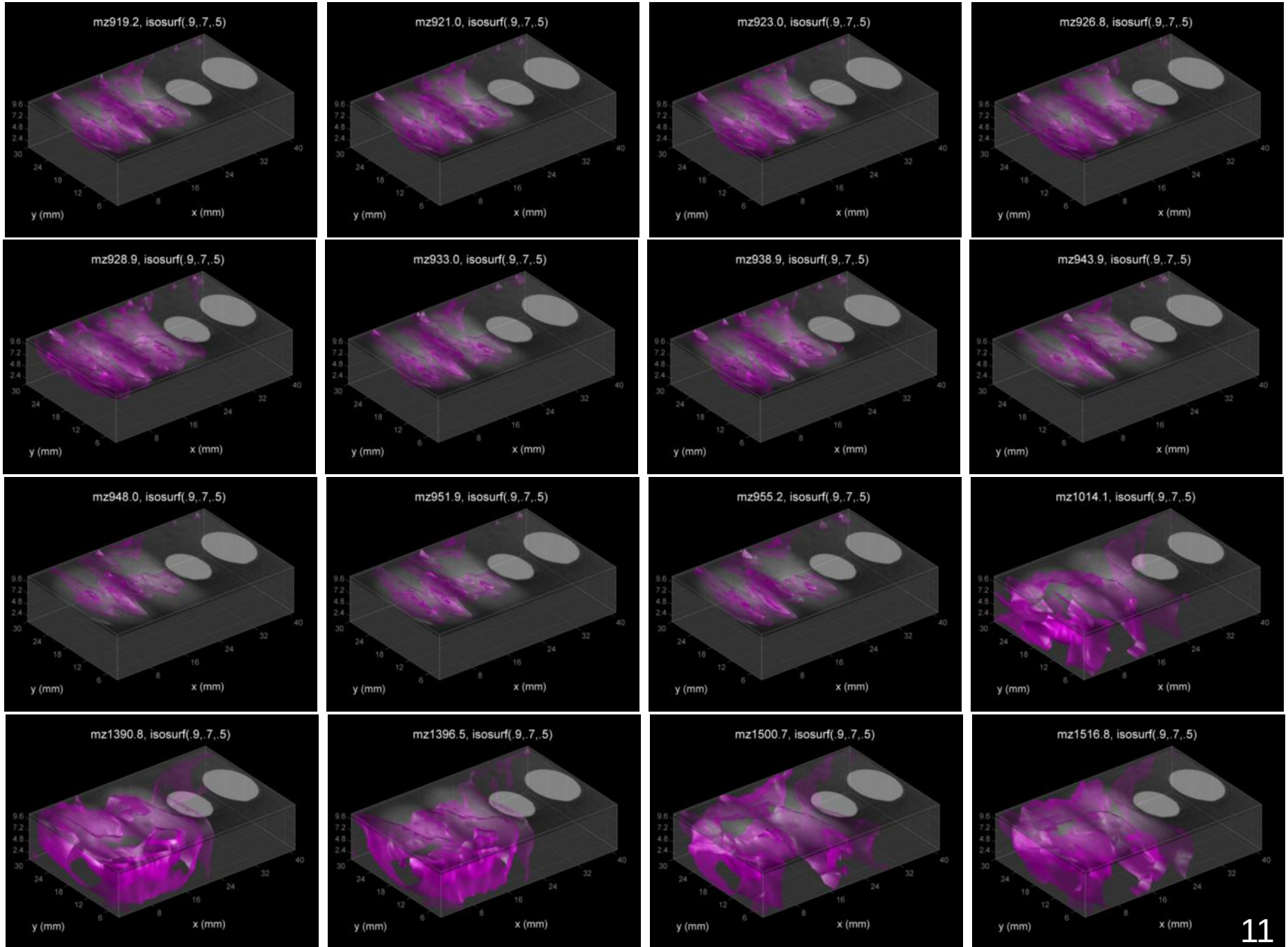

Figure S4: Additional mass signals from *C. albicans* ySN250 vs. *P. Aeruginosa PAO1*

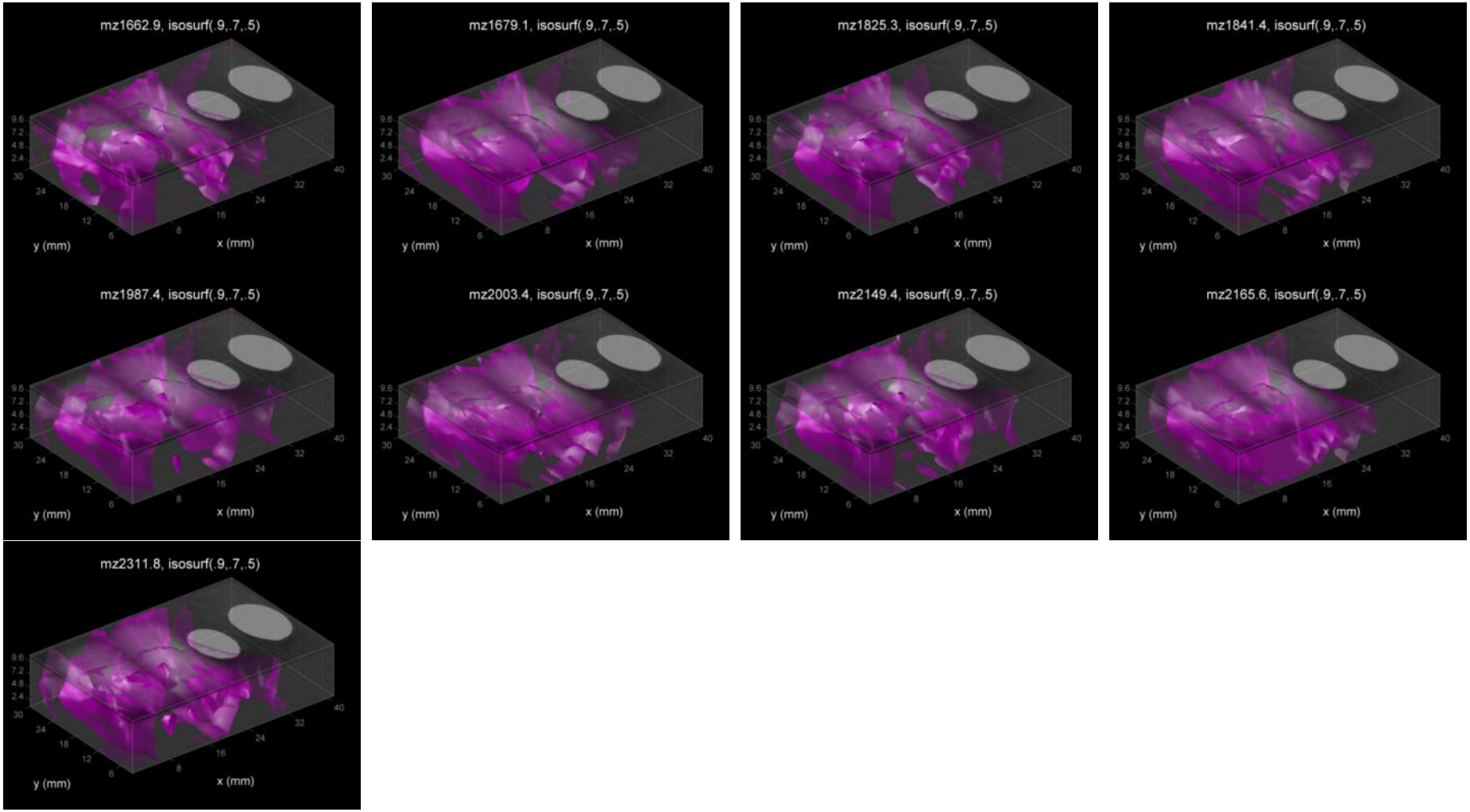

Figure S5: Annotation of MS2 spectrum for rhamnolipid at m/z 673

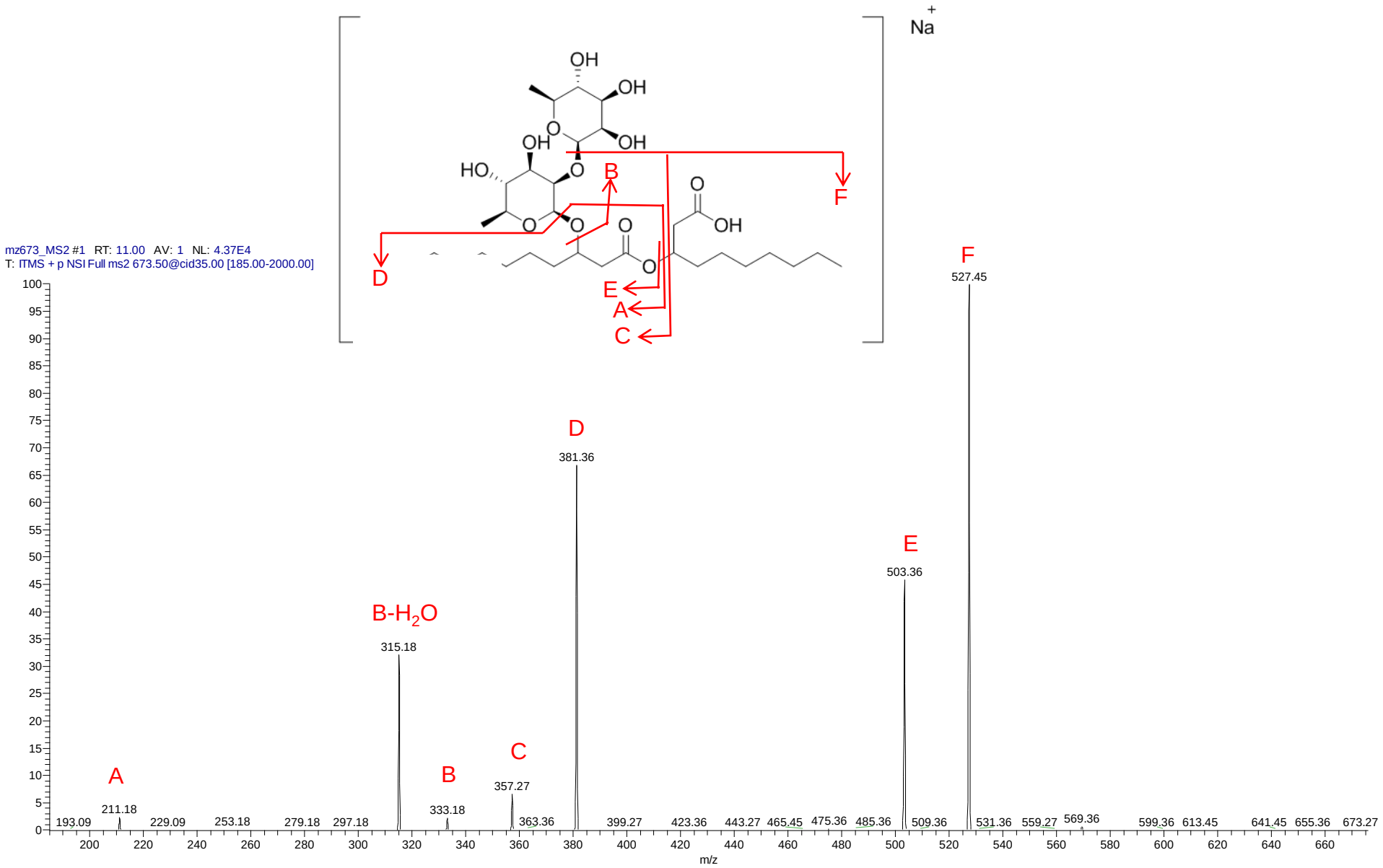

Description: Annotation of the CID MS2 spectrum for the rhamnolipid species at m/z 673.

Figure S6: Annotation of MS2 spectrum for rhamnolipid at m/z 699

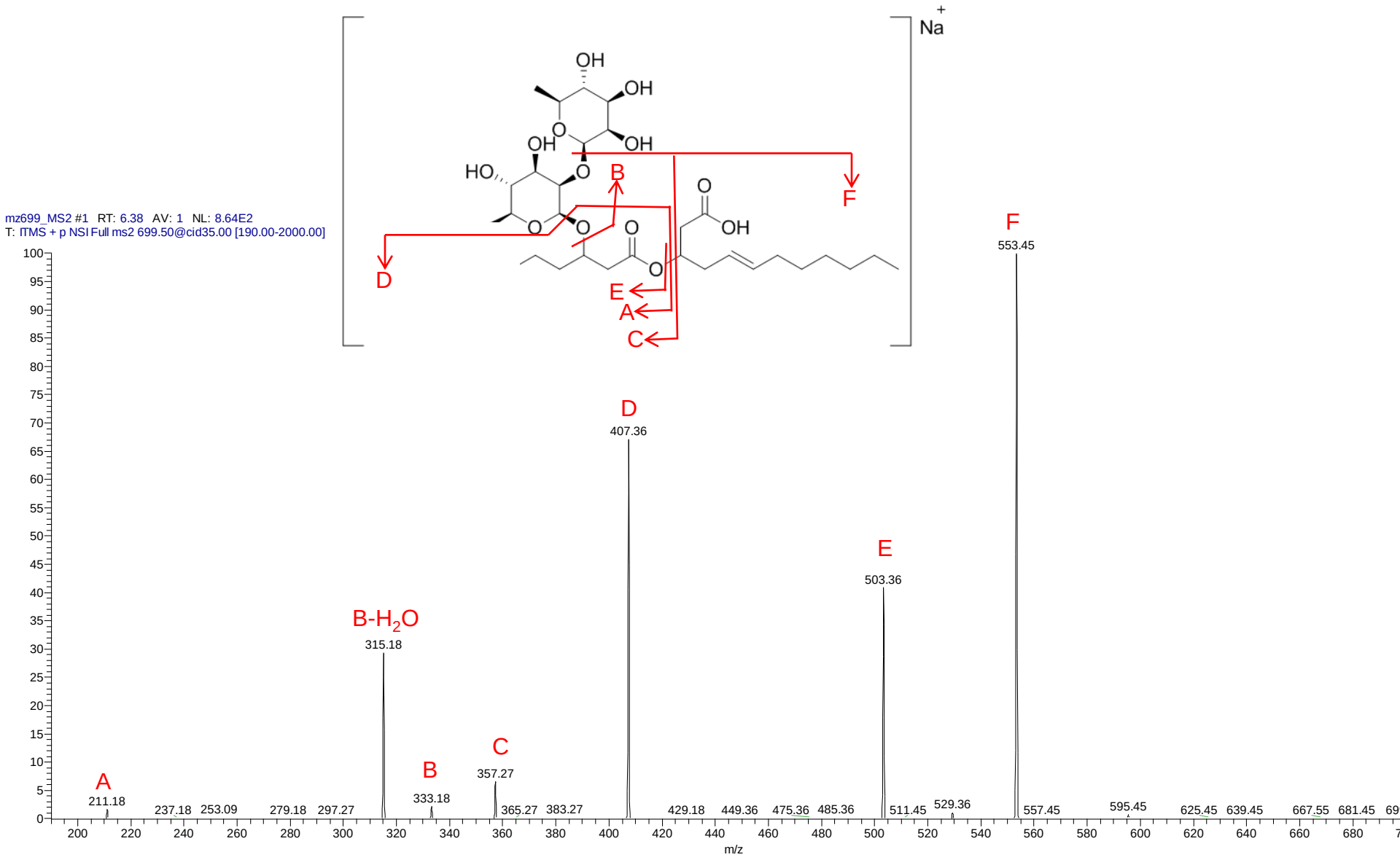

Description: Annotation of the CID MS2 spectrum for the rhamnolipid species at m/z 699.

Figure S7: Annotation of MS2 spectrum for rhamnolipid at m/z 701

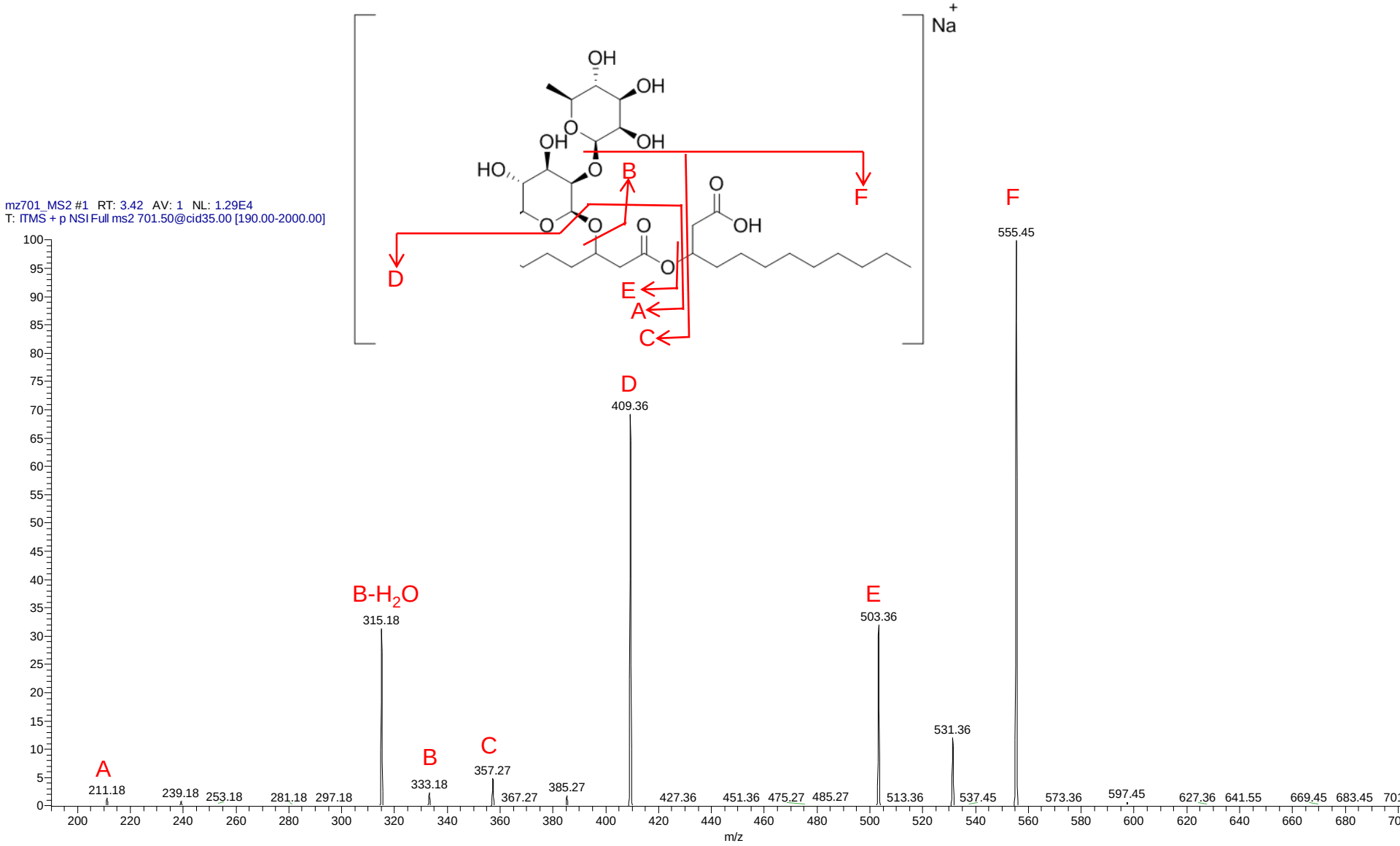

Description: Annotation of the CID MS2 spectrum for the rhamnolipid species at m/z 701.

Table 1: Annotation of NMR data for all 3 rhamnolipid species

Rhamnolipid atom numbering

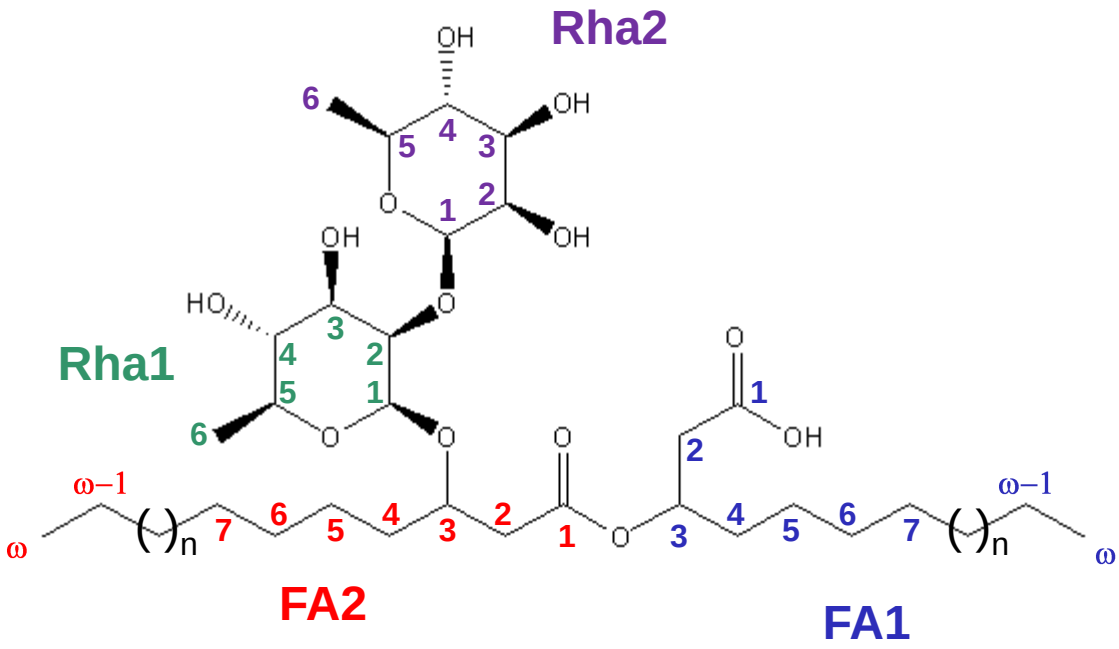

Description: Rhamnolipid atom numbering scheme used in Table 1 on following page.

Table 1: Annotation of NMR data for all 3 rhamnolipid species

		Sample A			Sample B						Sample C		
		Rha-Rha-FA (10:0) - FA (10:0) *m/z* = 673.3733 $[M+Na]^+$			Rha-Rha-FA (10:0) - FA (12:1) *m/z* = 699.4114 $[M+Na]^+$			Rha-FA (10:0) - FA (12:1) *m/z* = 553.3347 $[M+Na]^+$			Rha-Rha-FA (10:0) - FA (12:0) *m/z* = 701.4109 $[M+Na]^+$		
Residue	**Position**	**^{1}H (ppm)**	**J (Hz)**	**^{13}C (ppm)**	**^{1}H (ppm)**	**J (Hz)**	**^{13}C (ppm)**	**^{1}H (ppm)**	**J (Hz)**	**^{13}C (ppm)**	**^{1}H (ppm)**	**J (Hz)**	**^{13}C (ppm)**
FA-1	1	-		174	-		173.9	-		173.9	-		173.9
	2	2.56	d 7.0	39.9	2.56	d 7.5	39.7	2.54	d, 7.4	39.7	2.57	d, 6.9	39.8
	3	5.24	dt, 6.5	72.1	5.25	dt, 6.3	71.8	5.24	dt,6.3	71.8	5.24	dt, 6.3	72
	4a	1.62	m	34.9	2.36	dd, 7,14	32.1	1.62	m	34.8	1.62	m	34.8
	4b				2.43	dd, 6.5,14.5							
	5	1.32	m	26.1	5.36	m, 7.5,18.1	124.2	1.32	m	26.1	1.33	m	25.9
	6	1.27-1.36	m	30.3	5.53	m, 7.5,18.3	134.0	1.27-1.36	m	30.3	1.27-1.36	m	30.3
	7	1.27-1.36	m	30.3	2.06	dd, 7,14	27.8	1.27-1.36	m	30.3	1.27-1.36	m	30.3
	8	1.27-1.36	m	30.3	1.27-1.36	m	29.9	1.27-1.36	m	30.3	1.27-1.36	m	30.3
	midchain	1.27-1.36	m	30.3	1.27-1.36	m	29.9	1.27-1.36	m	30.3	1.27-1.36	m	30.3
	ω–2	1.28	m	32.8	1.31	m	32.3	1.28	m	32.8	1.27	m	32.7
	ω–1	1.31	m	23.6	1.32	m	23.2	1.31	m	23.6	1.31	m	23.6
	ω	0.89	t, 6.9	14.2	0.89	t, 7.0	13.8	0.89	t, 6.9	14.2	0.89	t 7.0	14.2
FA-2	1	-		172.2	-		171.9	-		171.9	-		171.9
	2a	2.48	dd, 5.6,15.3	41.1	2.48	dd, 5.9,15.3	41.1	2.48	dd, 5.9,15.3	41.3	2.48	dd, 5.6,15.1	40.8
	2b	2.56	dd, 7.3,9.7		2.58	dd, 6.7,15.2		2.58	dd, 6.7,15.2		2.57	dd 2.5,7.5	
	3	4.04	dt, 6.0	75.3	4.05	dt, 6.0	75.0	4.05	dt, 6.0	75	4.05	dt, 6.2	74.8
	4	1.54	m	25.7	1.54	m	33.9	1.54	m	33.9	1.55	m	33.9
	5	1.34	m	30.6	1.35	m	25.3	1.35	m	25.3	1.36	m	30.5
	6	1.27-1.36	m	30.3	1.27-1.36	m	30.3	1.27-1.36	m	30.3	1.27-1.36	m	30.3
	7	1.27-1.36	m	30.3	1.27-1.36	m	30.3	1.27-1.36	m	30.3	1.27-1.36	m	30.3
	midchain	1.27-1.36	m	30.3	1.27-1.36	m	30.3	1.27-1.36	m	30.3	1.27-1.36	m	30.3
	ω–2	1.28	m	32.8	1.27	m	32.8	1.27	m	32.8	1.28	m	32.7
	ω–1	1.31	m	23.6	1.32	m	23.6	1.32	m	23.6	1.31	m	23.6
	ω	0.89	t, 6.9	14.2	0.89	t, 7.0	14.2	0.89	t, 7.0	14.2	0.92	t 7.0	14.2
Rha-1	1	4.92	d, 1.2	98.8	4.92	d, 1.1	98.7	4.78	d, 1.6	100.2	4.92	d, 0.9	99
	2	3.73	dd, 1.7,3.3	80.3	3.73	dd, 1.7,3.3	71.7	3.73	dd, 1.7,3.3	71.7	3.73	dd, 1.7,3.3	80.3
	3	3.7	dd, 3.4,9.7	71.4	3.61	dd, 3.5,9.5	72.0	3.61	dd, 3.5,9.5	72	3.7	dd, 3.3,9.3	71.4
	4	3.3	obs by MeOD	73.7	3.35	obs by MeOD	73.7	3.35	obs by MeOD	73.7	3.32	t, 9.5	73.7
	5	3.63	dd, 6.3,9.7	69.8	3.65	dd, 6.2,9.6	69.8	3.65	dd, 6.2,9.6	69.8	3.63	overlapped	69.8
	6	1.22	d, 6.2	17.9	1.23	d, 6.1	17.8	1.23	d, 6.1	17.8	1.23	d 6.2	17.7
Rha-2	1	4.87	d, 1.6	104	4.88	obs by HOD	104.0	-		-	4.88	d, 1.6	104.1
	2	3.96	dd, 1.7,3.3	71.7	3.96	dd, 1.7,3.2	?	-		-	3.96	dd, 1.7,3.3	71.7
	3	3.64	dd, 3.2,9.5	72	3.64	dd, 3.4,9.6	?	-		-	3.66	dd, 3.3,9.4	72
	4	3.38	t, 9.5	73.8	3.35	t, 9.5	73.8	-		-	3.38	t, 9.5	73.8
	5	3.68	dd, 6.2,9.5	69.9	3.64	dd, 6.2,9.6	69.6	-		-	3.68	dd, 6.3,9.4	69.9
	6	1.24	d, 6.2	17.8	1.24	d 6.1	17.5	-		-	1.25	d 6.2	17.7

Description: Annotation of NMR data for observed rhamnolipid species. Refer to previous page for atom numbering scheme. Purified rhamnolipid species at m/z 673 contained ~10% of the single rhamnose variant. Purified rhamnolipid species at m/z 699 contained ~12% of saturated species as well as the single rhamnose variant of the unsaturated species (m/z 553). Purified rhamnolipid species at m/z 701 contained ~15% of the unsaturated m/z 699 species as well as the single rhamnose variant. Also, species at m/z 701 showed two different resonances for the terminal methyls of the fatty acids which were arbitrarily assigned to different fatty acid residues as NMR could not distinguish which fatty acid they belonged to. NMR spectra were acquired at 600MHz and 298K in methanol-d4. Chemical shifts were referenced to the residual methanol methyl resonance at 3.31ppm.

Figure S8: Comparison of ^{1}H NMR spectrum for all 3 Rhamnolipid species

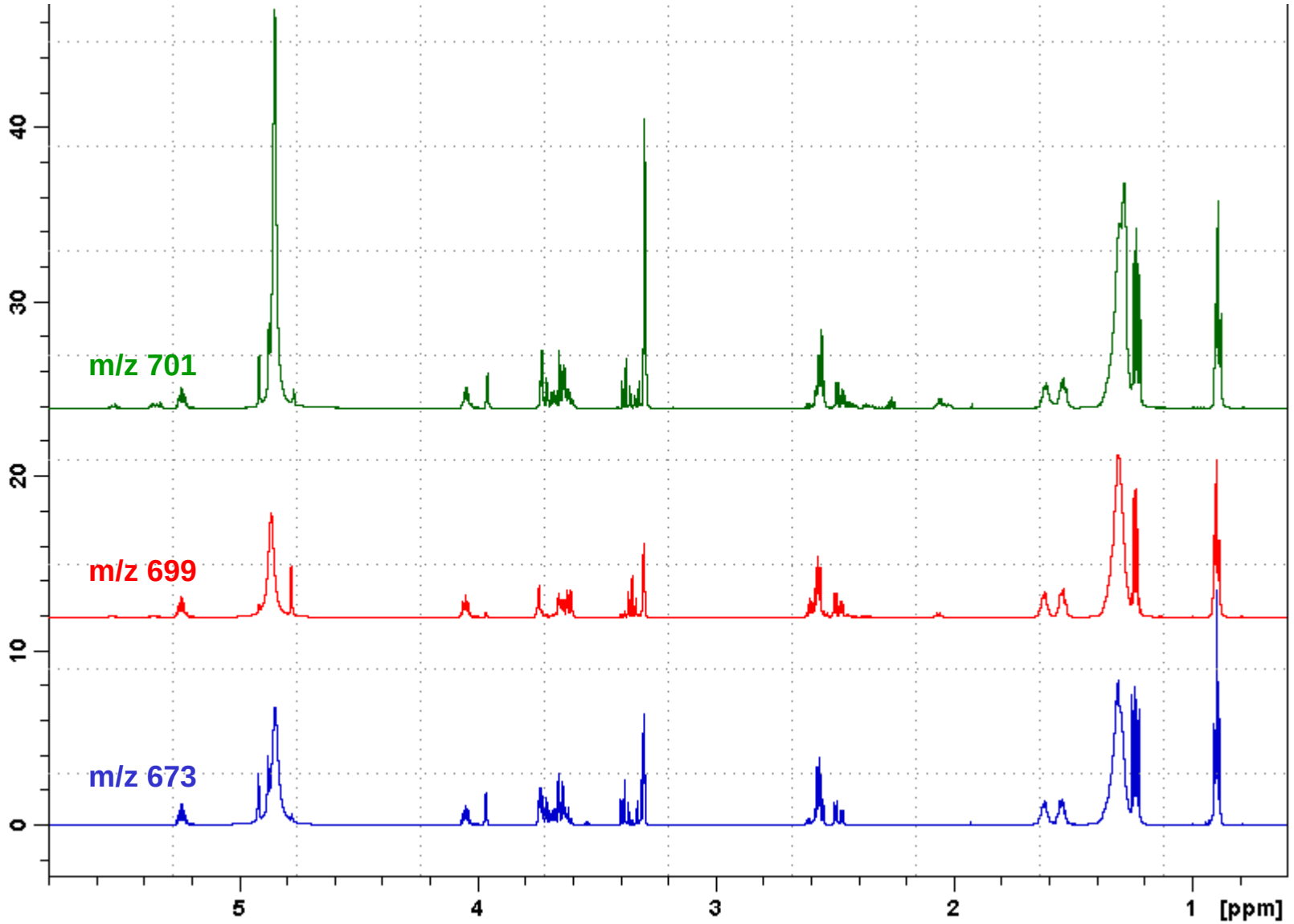

Description: Overlay of the ^{1}H NMR spectra for all 3 main rhamnolipid species observed. NMR spectra were acquired at 600MHz and 298K in methanol-d4. Chemical shifts were referenced to the residual methanol methyl resonance at 3.31ppm.

Figure S9: Example annotation of ^{1}H NMR spectrum (for m/z 673 species)

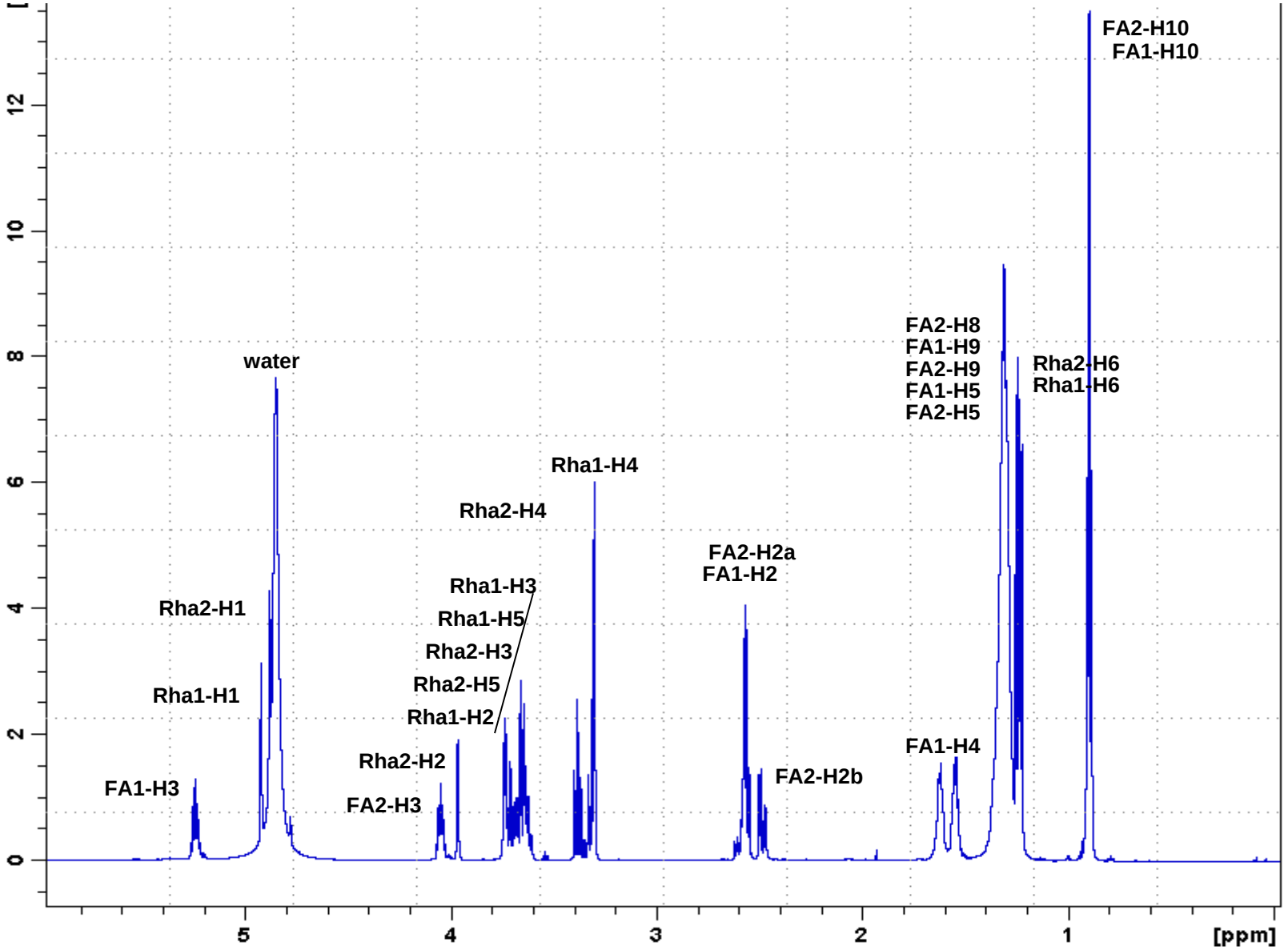

Description: Example annotation of the ^{1}H NMR spectrum for the rhamnolipid species at m/z 673. NMR spectra were acquired at 600MHz and 298K in methanol-d4. Chemical shifts were referenced to the residual methanol methyl resonance at 3.31ppm. Refer to page 7 for atom numbering scheme.

Figure S10: Evidence for double bond location for rhamnolipid species at m/z 699

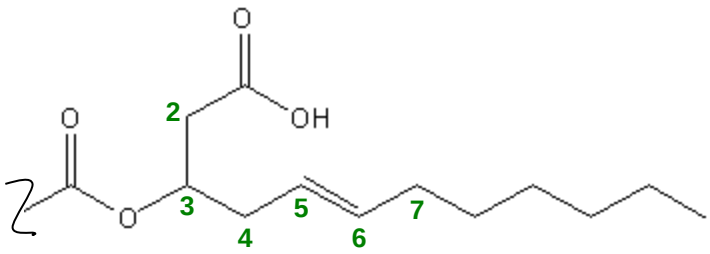

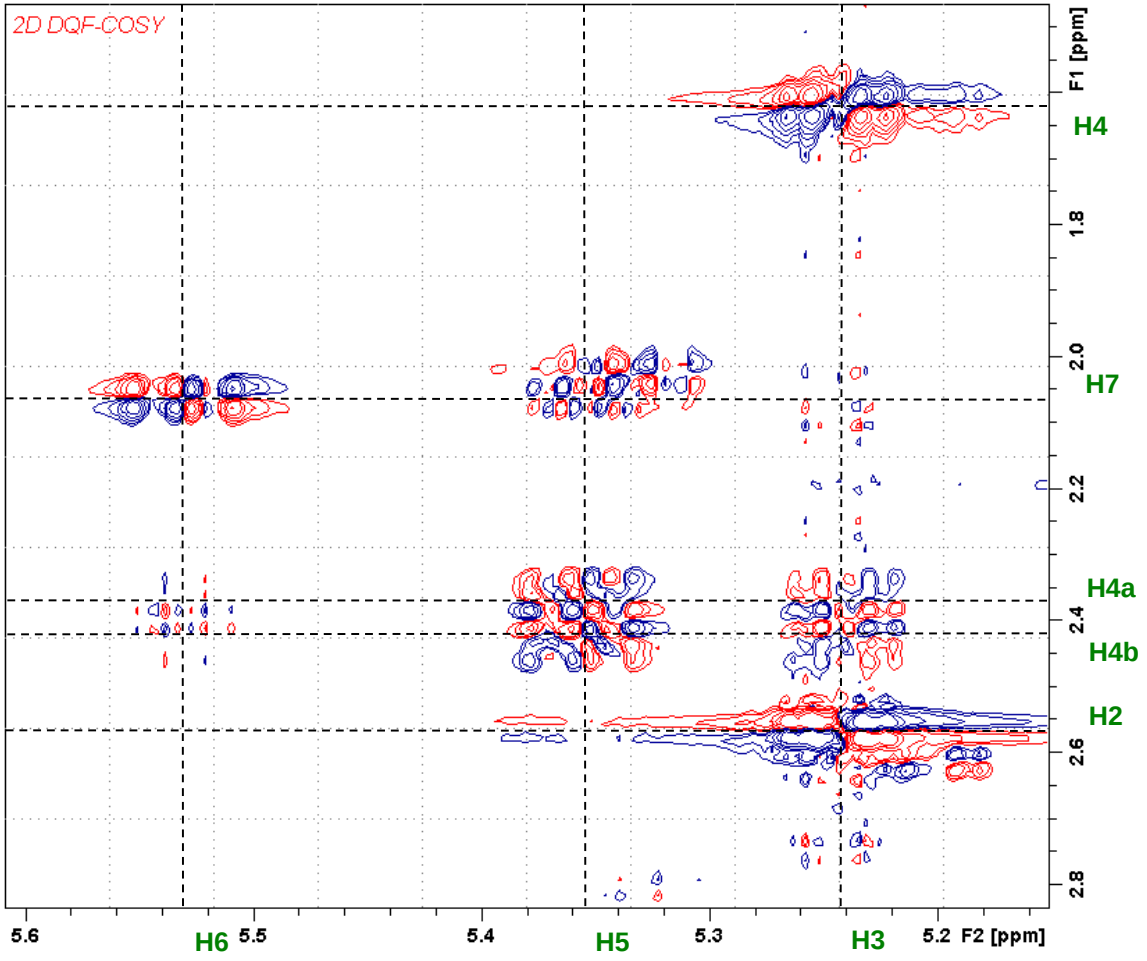

Description: Evidence for the double bond of the rhamnolipid species at m/z 699 being located at carbon 5 on fatty acid chain 1 (see page 7) are as follows: FA1-H3 has a unique chemical shift at 5.25ppm, FA1-H3 shows coupling to H2 and H4, FA1-H4 resonance of unsaturated species is 1.6ppm while resonance of saturated species (m/z 701) shows two resonances for H4 near 2.4ppm. NMR spectra were acquired at 600MHz and 298K in methanol-d4. Chemical shifts were referenced to the residual methanol methyl resonance at 3.31ppm.